Free-standing Nanometer-Thick Covalent Organic Framework Films for Separating CO_2 and N_2

Masaki Kato[1], Ryo Ota[2], Takashi Endo[2], Takashi Yanase[3], Taro Nagahama[1,4],*

*Toshihiro Shimada[1,4]**

[1] Graduate School of Chemical Science and Engineering, Hokkaido University, Kita 13 Nishi 8, Kita-ku, Sapporo 060-8628, Japan

[2] Center for Advanced Reseearch of Energy and Material, Faculty of Engineering, Hokkaido University, Kita 13 Nishi 8, Kita-ku, Sapporo 060-8628, Japan.

[3] Department of Chemistry, Faculty of Science, Toho University, Miyama 2-2-1, Funabashi 274-8510, Japan

[4] Division of Applied Chemistry, Faculty of Engineering, , Hokkaido University, Kita 13 Nishi 8, Kita-ku, Sapporo 060-8628, Japan

Graphical abstract

Abstract

Covalent organic frameworks (COF) have been gathering much attention because the shapes, sizes and chemical functions of their nanostructured pores can be arbitrarily controlled by designing the organic precursors. We fabricated cm-size free-standing COF films with the thickness of 50-100 nm by an alternating vacuum deposition polymerization method. Precise adjustment of the stoichiometry by digitally controlled deposition was essential for producing the robust free-standing COF films. High-resolution electron microscopy revealed 3-nm pore structures which correspond to the atomic structure of the COF. Small angle x-ray diffraction shows the existence of a similar periodicity. The CO_2-N_2 gas phase separation properties were evaluated from 10^3-10^5 Pa and the parameters for each molecular permeation were determined. Based on the detailed analysis, it was found that the selectivity comes from the greater sorption affinity of CO_2 to the COF compared to N_2, which is consistent with the quantum chemical calculation. Since the vapor phase method can be used to coat various shaped templates, our method provides a new option for fabrication of neat COF membranes with various structures and their applications for the separation membrane.

Keywords

covalent organic frameworks, free-standing film, vacuum deposition polymerization, high resolution electron microscopy, CO_2 separation membrane

Introduction

There is a general concern about the impact of climate change caused by global warming on the natural, biological, and human environments. The increase of the CO_2 concentration in the atmosphere is suspected as the primary cause. The development of technology to separate and capture CO_2 is highly desired.[1] Membrane separation technology is regarded as a promising approach for the CO_2 separation because of its high energy efficiency, low cost and flexibility in the facility design.[2] The mixed matrix membrane (MMM) is expected to overcome the Robeson upper bound of conventional polymeric membranes, *i.e.*, trade-off between gas permeation and selectivity.[3-6] However, improvement of the permeation and separation performance of MMM composites[7,8] have an intrinsic upper limit because the influences of the grain boundaries of the fillers dispersed in the matrix cannot be avoided. Thus, tremendous efforts have been made to prepare defect-free membranes by using new materials, such as zeolites,[9,10] MoS_2-ionic liquid,[11] metal-organic frameworks[12,13] and covalent organic frameworks (COF).[14–16]

The COF is a new organic material group with periodically distributed pores, which is synthesized by arranging highly symmetrical organic building blocks into the two-dimensional or three-dimensional frameworks.[17-19] COFs have a crystallinity, high porosity, tunable pore characteristics, and high thermal and chemical stability. With these features, COFs are expected for applications in adsorption,[20-24] electrode materials of Li ion batteries,[25] catalysts for CO_2 reduction,[26-29] and separation membranes.[30-34]

In order to apply COFs for separation membranes, it is necessary to fabricate thin films with an excellent processability. The current procedures use powder form COFs synthesized by organic processes with embedding in the MMM[35-37], or using reactions such as solvothermal ones with

immersed substrates,[38,39] or in continuous flows,[40,41] at liquid-liquid interfaces,[30,31.33.42] at air-liquid interfaces,[43,44] or in a monomer-exchange process.[45] However, these methods have the following problems:

(1) Gas permeation and separation performances decrease with an increase in the COF loadings because the compatibility between the COF and MMM becomes low.

(2) It is impossible to use the solvothermal or the continuous flow methods to fabricate free-standing films because these methods must use substrates to grow the films.

(3) Although it has been reported that free-standing films can be obtained by using the reaction at the liquid-liquid interfaces, the air-liquid interfaces or in monomer-exchange process, it is very difficult to precisely control the film thickness. There is also a problem of the inclusion of the solvents as impurities in the films.

In order to solve these problems, we focused on a method to fabricate the COF films from a vapor phase. The vapor phase synthesis of COFs has been reported for a few-molecular-layer COFs on single crystalline metal substrates for scanning tunneling microscopy (STM) observations.[46-48] However, these films could not be used for practical membrane-based devices because they were on the metal substrates and were not continuous on a large scale.

The difficulty in the deposition polymerization is the stoichiometry control and the removal of the substrate. We solved these problems by alternating the deposition of the precursors on a dissolvable substrate with precise control of the thickness of each layer followed by annealing. Our goal here is to prepare free-standing COF films and evaluate the CO_2/N_2 gas permeation properties. The free-standing films have great potentials for membrane separation because they can be incorporated into high-flux hollow fiber membranes. The obtained films were fully characterized and the CO_2 and N_2 gas permeation properties were evaluated.

Experimental Section

Fabrication of COF films

We fabricated COF films with an imide-bonding network structure from (1,3,5-tris(4-aminophenyl)benzene (TAPB) and naphthalene-1,4,5,8-tetracarboxylic dianhydride (NTCDA) precursors (Fig. 1a). It is usually difficult to synthesize polymer films with a precisely controlled thickness and stoichiometry by using deposition polymerization from the vapor phase. In order to solve these problems, we developed a new apparatus (Fig. 1b) to alternatingly deposit TAPB and NTCDA on substrates with real-time thickness monitoring by a quartz crystal microbalance (QCM) and automatic source control. Figure 1c schematically illustrates the overall COF film fabrication. A pre-designed amount of NTCDA was deposited on the substrate, then the source was switched to TAPB and the deposition was continued.

In greater detail, the alternating deposition was done in a vacuum chamber evacuated by a turbo molecular pump (TMP) to a pressure below 5.0×10^{-4} Pa. The precursor materials, TAPB (>93.0%) and NTCDA (>99.0%), were purchased from Tokyo Kasei and used without further purification. Approximately 100 mg of NTCDA and TAPB were introduced in separate quartz crucibles, then fixed on a carousel at the bottom of the chamber. The precursors were sublimed by a lamp heater and deposited on the substrate (Si/SiO_2 or KCl (001) polished surface (OHYO KOKEN KOGYO Co., Ltd., Tokyo, Japan)) placed 5 cm above the deposition source.[49] The substrate was rotated at 20 rpm to enhance the uniformity of the films. The amounts of the deposited precursors were monitored by changes in the frequency (Δf) of the QCM (INFICON, 6 MHz). The QCM was maintained at about 17 °C by water circulation in order to avoid desorption of the precursor from

the QCM surface and to prevent thermal deviation of the QCM frequency. The thickness-Δf relationship was calibrated by measuring the thickness of the deposited films of each precursor by laser microscopy (KEYENCE VX-8700). First, NTCDA was deposited on the substrate. The carousel was then rotated and TAPB was deposited on the substrate. Rotation of the precursor carousel and the intensity of the lamp heater were automatically controlled by a computer program that monitors the QCM. The deposition rate of the precursors was 0.1 nm s^{-1}. By repeating these operations for 25-100 times, the alternating deposited film was prepared.

The film after the alternating deposition was removed from the chamber and annealed under vacuum conditions (<10 Pa) in a glass tube in order to facilitate the imide forming reaction between the precursors to prepare the COF films. This annealing causes partial desorption of the precursors and the optimal ratio of the precursors in the as-deposited films was dependent on the annealing conditions as explained in the Results and Discussion.

Characterization of the COF films

Fourier transform infrared spectroscopy (FTIR) was performed using a JASCO FT/IR-4700 with a 4 cm^{-1} resolution. The COF films and the precursor powders were measured by the transmission method on the KCl substrate and the attenuated total reflection method, respectively. Scanning transmission electron microscopy (STEM) was performed using an aberration-corrected FEI Titan3 G2 60-300 at the acceleration voltage of 60 kV. The small angle X-ray scattering (SAXS) measurement was conducted using a Rigaku Nano-viewer IPA with the exposure time of 4.5 h. A KEYENCE VX-8700 laser microscope was employed to measure the film thickness using the step between the film and the substrate. It was also used for observation of the free-standing films.

Gas permeation measurements

Gas permeation measurements were conducted using the apparatus shown in Fig. S1 based on the differential-pressure methods (ISO 15105-1:2007). Details of the measurements are described in the Supporting Information. Briefly, the apparatus consisted of two chambers, a gas manifold and a partial pressure measurement chamber equipped with a calibrated pressure gauge and a quadrupole mass spectrometer (QMS). The COF film was fabricated on a KCl (001) single crystal substrate and the sample was gently placed in water. The KCl then dissolved and the COF film floated on the surface. Next, the free-standing film was lifted off by a porous Al_2O_3 support (Whatman® Anodisc Membrane Filters, 13-mm diam., 0.02-μm pore size). The COF film on the support was dried in an ambient atmosphere, then glued onto a separator with a NW-KF25 flange by a vacuum-compatible epoxy resin (Stycast 2850G). The COF separator was positioned between a supply gas manifold and the partial pressure measurement chamber. Residual gas on both sides was removed to achieve a vacuum better than 5×10^{-5} Pa by TMP pumping for over 12 h. The pressures of the feed and permeate gases were measured by a capacitance gauge (CANON ANELVA, M342DG-13) and a crystal-and-cold-cathode combination gauge (Tokyo Electronics Co., cc-10). The gas components in the permeate side were determined by a QMS (INFICON, Transpector2) with differential pumping. All the measurements were repeated at least three times and graph plots and error bars show the average and standard error of the experiments, respectively. The procedure and formulas used for calculating the permeance, ideal selectivity, and separation factor are explained in the Supporting Information.

Results and Discussion

Preparation and Characterization of COF films

First, we explain the results of the film preparation. Figure S2 shows the recorded decrease in the QCM frequency, which corresponds to the deposited amount of TAPB and NTCDA. The stepwise decrease at 16 and 9 Hz each indicates that the cycle was successfully controlled. The thickness of each layer was set at 1-2 nm and no significant difference in the film structure and properties were observed by changing this parameter. Precursors were repeatedly deposited from 25 to 100 times to fabricate an alternatingly deposited film. The film was annealed in a vacuum to facilitate the imide-forming reaction between TAPB and NTCDA. We performed many experiments with different monomer ratios, annealing temperatures and annealing periods for the prescreening. We found that these factors are interconnected with each other, *i.e.*, the optimum stoichiometry can be achieved under different annealing condition by adjusting the monomer ratio. In the following section we explain the results of two types of COF films with the upper limit and lower limit for obtaining films with a high quality (FTIR-based) as shown in Table 1. The conditions were optimized by controlling three parameters, *i.e.*, the deposition ratio (weight ratio) of TAPB and NTCDA, temperature and time during annealing in a vacuum. Since partial evaporation occurred during the vacuum annealing, stoichiometry control requires optimization of the precursor ratio depending on the annealing conditions. This was done using FTIR as described in the following table.

Table 1. Conditions to fabricate two types of COF films

Sample name	TAPB : NTCDA deposition ratio	Annealing temperature	Annealing time
"HTA"(high temperature annealed)	1 : 1.2	400 °C	10 min

"LTA" (low temperature annealed)	1 : 2.5	275 °C	12 h

Figure 2a shows the FTIR spectra of the film with the ratio TAPB : NTCDA = 1 : 1.2 annealed at various temperatures including those of an as-deposited film and each precursor. The "+" symbols denote the peaks from unreacted species (3353 cm^{-1} and 1607 cm^{-1} from $-NH_2$ of TAPB, 1781 cm^{-1} from C=O of NTCDA), whereas "x" denotes those from the imide bonded species (1714 cm^{-1} and 1673 cm^{-1} from symmetric and asymmetric vibrations of C=O, respectively; 1344 cm^{-1} from -C-N-C stretching[50]). As the imide-forming reaction was completed, the "+" peaks disappeared and the "x" peaks became relatively strong. It is noted that the total absorption intensity decreased due to desorption of the precursor molecules that occurred during the annealing. Figure 2b shows the FTIR spectra with the same annealing conditions (400 °C, 10 min, high temperature annealed (HTA)-COF afterwards) of the precursor films but with various TAPB : NTCDA ratios. It was found that the "+" peaks of the unreacted precursors disappeared when the ratio was TAPB: NTCDA=1:1.2. This result shows that the optimum precursor ratio is dependent on the annealing conditions. By using the same procedure (Fig. S3), the optimum annealing condition for the precursor ratio of TAPB : NTCDA =1 : 2.5 was determined to be 275 °C for 12 h (low temperature annealed (LTA)-COF).

Free-standing COF films were prepared by alternating the depositing precursors on water-soluble KCl substrates followed by annealing, then dissolving the substrates in water. They were obtained as a floating object on the water surface as shown in Fig. 3a. The film can be lifted out and transferred to any substrates from the water surface. Figure 3b shows an optical image of the COF film placed on a metal ring to partly cover the hole, in which the center part of the film was not supported by anything. Figure 3c shows a laser microscope image of the COF film on the Si

substrate. An interference fringe of the laser light was observed due to the deviation in the air gap thickness, which shows the smoothness and uniformity of the film. Figure S4 shows optical images of the COF films transferred to various substrates including sapphire, glass, and porous Al_2O_3 supports obtained by using the same method.

STEM and SAXS

Nanostructures of the free-standing COF films were evaluated by HR-STEM with atomic resolution. Figure 4a shows a STEM image of the HTA-COF film transferred on a TEM grid, which shows the typical overall structure of the HTA film. At a higher magnification, we found a randomly oriented network structure (Fig. 4b). Pore structures with the size of 2.4-3.6 nm were clearly identified in Fig. 4c by magnifying a part of Fig. 4b. This pore size is close to that of a previously reported prediction (2.9 nm) of the COF synthesized from the same precursors.[50]

On the other hand, we could not find a pore structure in the LTA-COF films from the STEM observations (Fig. S5). The difference between the HTA- and LTA- COFs is in accordance with previous reports, which has shown that the morphology of the COFs was dependent on the monomer concentration during the synthesis.[51] It was also reported that a low temperature reaction causes poor formation of the networking pore structures.[52] The present result indicated that the monomer ratio and the annealing conditions are important to finely tune the network structure of the COFs during the alternating deposition. The SAXS pattern of the free-standing HTA-COF films (Fig. 4d) showed a broad peak. The peak top placed at q = ca.1.5 nm^{-1} corresponding to the spacing of $\sqrt{3}/2q$ =3.6 nm for the hexagonal lattice, which was a slightly greater size than the (100) spacing of the bulk COF.[50] We consider this enlargement is due to the warping and entanglement of the layers, which is consistent with the gas permeation results.

The absolute thickness of the COF films grown directly on Si wafers was calibrated by a laser microscope (Fig. S6(a)). The thickness was consistent with the AFM measurement using partial scraping method (Fig. S6(b)). The thickness linearly increased with the repetition number. Annealing caused a decrease in the thickness by the factor of 0.52 (for HTA; 0.42 for LTA (the plot is not shown)), while the linearity with the repetition number was maintained. This thinning was due to sublimation of the unreacted precursors. It has been revealed that COF films whose thickness were precisely controlled on a nm scale can be fabricated by an alternating deposition.

The chemical stability of the HTA-COF films was evaluated by immersing the films in concentrated HCl aq. (12 M), NaOH aq. (1.3 M), toluene, tetrahydrofuran (THF), ethanol (EtOH), dichloromethane (CH_2Cl_2) and acetone for 24 hours. The FTIR peaks characteristics of the imide-bonding were maintained even after immersing the films in those chemicals (Fig. S7). This result indicated that COF films had high stabilities against acids and organic solvents, because the networking structure composed by the imide-bonding reinforced the chemical stability. The COF showed a relatively low resistivity for NaOH(aq) because the imide-bonding was hydrolyzed by a base.[53]

N_2 and CO_2 Gas Permeation and Separation

The gas separation properties of the free-standing COF films were characterized by a permeation test using an apparatus with a quadrupole mass spectrometer (QMS) and capacitance manometers. It was estimated that the film thickness of the HTA- and LTA- COF were ca. 50 and 100 nm, respectively, from the sample prepared under the same experimental conditions shown in Fig. S6(b). The examined gas species were pure CO_2, pure N_2 and CO_2/N_2 mixture (1 : 1) (see Supporting Information and Fig. S1). The COF membranes were supported by a porous Al_2O_3

membrane to make them tolerant to the pressure difference. The effect of the Al_2O_3 supports was negligible as explained in the Supporting Information.

Figure 5 shows the CO_2 or N_2 permeances and CO_2/N_2 ideal selectivity for the HTA-COF film of the CO_2 or N_2 pure gas that permeated through the film at the transmembrane pressures of 10^3 to10^5 Pa. When the transmembrane pressure was 10^5 Pa, the difference between CO_2 and N_2 was the highest. The permeance of CO_2 and N_2 was 1.79×10^{-8} mol m^{-2} Pa^{-1} s^{-1} and 0.39×10^{-8} mol m^{-2} Pa^{-1} s^{-1}, respectively. Thus, the ideal CO_2/N_2 selectivity at 10^5 Pa was calculated to be 4.58 (Table 2). The pore size of HTA-COF ranged between 2.4 and 3.6 nm based on the STEM observations, which is far greater than the kinetic diameters of CO_2 and N_2 (0.33 and 0.36 nm, respectively).[54] Based on this result, it is presumed that the CO_2/N_2 selectivity is not due to a molecular sieving effect but to differences in the solution-diffusion mechanism between CO_2 and N_2 in the films.

When the transmembrane pressure was 10^5 Pa, the CO_2 and N_2 permeance of the LTA-COF film was 5.7×10^{-10} mol m^{-2} Pa^{-1} s^{-1} and 1.2×10^{-10} mol m^{-2} Pa^{-1} s^{-1}, respectively (Table 2). These values are lower than the CO_2 and N_2 permeances of the HTA-COF film by factors of 31.4 and 32.5 times, respectively. This tendency, *i.e.*, in which the LTA-COF film permeance is lower than that of the HTA-COF film, was observed at all the measured transmembrane pressures (10^3-10^5 Pa) (Fig. S8). We consider the mechanism for this difference to be due to the HTA-COF films having partially oriented pores which formed a short gas permeation paths as determined by STEM, whereas the LTA-COF films did not have these paths.

We next measured the CO_2/N_2 separation factor of the HTA-COF films using the CO_2/N_2 mixture (molar ratio=1:1). There were no significant differences between the CO_2/N_2 separation

factor and CO_2/N_2 ideal selectivity for the HTA-COF film at the transmembrane pressures of 10^3-10^5 Pa (Fig. S9).

It is suggested from the results that a diffusion effect was dominant in the HTA-COF films due to the partially oriented pores. This model is in agreement with the fact that the value of the CO_2-N_2 separation factor for the HTA-COF film (4.66) was approximately in agreement with that of the CO_2/N_2 ideal selectivity (4.58). In addition, it was noted that the HTA-COF film had almost no contribution of a molecular gate effect[55], in which N_2 was prevented from permeating when the adsorption sites on the pore wall were occupied with CO_2.

On the other hand, the values of the CO_2/N_2 separation factor of the LTA-COF film (3.83) was lower than that of the CO_2/N_2 ideal selectivity (4.79). This indicated that the adsorption and solution effects played important roles during the permeation through the LTA-COF films. The mechanism is that the diffusion is hindered in the LTA-COF films due to the lack of ordered structures.

Table 2. CO_2 and N_2 permeance, CO_2/N_2 ideal selectivity and CO_2/N_2 separation factor of HTA-, LTA- COF films and Al_2O_3 support at the transmembrane pressure=10^5 Pa

	CO_2 permeance [a]	N_2 Permeance [a]	CO_2/N_2 ideal selectivity	CO_2/N_2 separation factor
HTA-COF film	1.8±0.2	0.39±0.04	4.6±0.8	4.7±0.3
LTA-COF film	0.057±0.004	0.012±0.002	4.8 ± 0.9	3.8±0.4
Al_2O_3 support	142 ± 2	133 ± 0.4	1.06±0.02	1.54±0.02

[a] Unit: 10^{-8} mol m^{-2} Pa^{-1} s^{-1}

DFT calculations

In order to further understand the gas permeation processes of the COF films, we conducted DFT-D calculations using Gaussian16.[56] We calculated the interaction energies (ΔE) between the gas molecules and functional groups of the COF (see Supporting Information). The calculations predicted that the adsorption site of the gas molecules in the COF was the O atom of the imide group (Fig. 6). Interestingly, CO_2 adsorbed onto the site at the distance of 2.84 Å which was much closer than that of N_2 (3.25 Å). The calculations also predicted that the COF has higher affinities to CO_2 than N_2 at the ΔE of -17.2 kJ mol^{-1} vs. -9.0 kJ mol^{-1}, which are consistent with the experimental isosteric heat of adsorption from a previous report.[50]

Mechanism of gas permeation through the COF films

The mechanism of gas permeation through a COF film has not been discussed by applying quantitative model parameters, probably because it has been difficult to use well-defined and uniform samples. We employed the partial immobilization model with dual mode sorption used in glassy polymer membranes.[57,58] The mechanism of the gas permeation through the glassy polymer is generally explained by using a solution-diffusion mechanism with the dual mode sorption model and partial immobilization model.

Based on these models, the gas concentrations inside the film are the sum of the Hrenry sorption (to matrix region) and Langmuir sorption (to microvoid region). The gas diffusivity in the films is described by a mixture of diffusivities in those regions at a certain ratio.

Table 3 and Fig. 7 show the fitting results. The parameters were determined by a numerical solution and experimental gas permeation data using a least-square genetic algorithm fitting (see details in Supporting Information). The HTA-COF film had higher k_D, C_H', and b for CO_2 (8.45×10^{-5}, 1.0×10^{5}, and 3.51×10^{-5}, respectively) values than those for N_2 (1.0×10^{-5}, 8.56×10^{4},

1.0×10^{-5}). It shows that the HTA-COF film has a greater solubility of CO_2 than that of N_2 in both the matrix and void region, which is consistent with the DFT result of the greater interaction energy of CO_2 than that of N_2 in the imide groups of COF.

The *b* values of CO_2 and N_2 in the HTA-COF films were in the range of 10^{-5} to 10^{-4} Pa^{-1}, which indicated that at the high feed gas pressure, pores in the COF film were saturated by gas molecules, and the gas permeation through the films was governed by a Henry sorption mechanism. The *b* values of the LTA-COF film were not significantly different from those of the HTA-COF film whereas the k_D and C_H' of the LTA-COF film were much higher and lower than those of the HTA-COF film, respectively. These results suggested that gas molecules in the LTA-COF film were more easily adsorbed in the matrix region than in the void region because the LTA-COF film was structureless.

In both the matrix and void regions, the diffusion coefficient of the HTA-COF film was much greater than that of the LTA-COF film. Thus, it was estimated that the pore structures in the HTA-COF film worked as diffusion pathways for the gas molecules. The absence of so-called gating effects in our results, in which CO_2 blocks the permeation of N_2, is explained as follows. The pore size of our COF is greater than the molecular size even with the entanglement and interpenetration and that the N_2 permeation is not blocked by adsorbed CO_2. Designing and synthesizing COF membranes with the narrower pore size will realize the gating effects and interesting functions of the separation films.

The discussion above can be summarized as follows:

1. Both the matrix (solvation of gas to the polymer followed by diffusion) and void (diffusion on the channel surface) contribute to the selectivity.

2. The selectivity comes from the stronger interaction between CO_2 and the polymer, which increases both the matrix and void diffusion.

3. The difference in the selectivity and the permeation between HTA-COF and LTA-COF comes from the ordering of the void channel which is consistent with the STEM images.

4. The "gating effect" was not observed because the void size is much greater than the CO_2 or N_2.

Table 3 Dual mode sorption and partial immobilization parameters for HTA- and LTA- COF films

Film	Gas	k_D [i]	C_H' [ii]	b [iii]	D_D [iv]	D_H [v]
HTA	CO_2	8.47×10^{-5}	1.00×10^{5}	3.51×10^{-5}	2.14×10^{-12}	2.61×10^{-16}
	N_2	1.00×10^{-5}	8.56×10^{4}	1.00×10^{-5}	8.37×10^{-12}	1.31×10^{-15}
LTA	CO_2	1.67×10^{-2}	5.92×10^{3}	1.00×10^{-4}	8.63×10^{-16}	6.99×10^{-22}
	N_2	1.64×10^{-3}	1.04×10^{3}	4.89×10^{-5}	2.73×10^{-15}	2.45×10^{-19}

i Henry's law constant. Unit: mol m^{-3} Pa^{-1}

ii Langmuir capacity. Unit: mol m^{-3}

iii Langmuir affinity constant Unit: Pa^{-1}

iv Diffusion coefficient in the matrix region Unit: m^2 s^{-1}

v Diffusion coefficient in the void region Unit: m^2 s^{-1}

Conclusion

This study is the first report about the preparation of free-standing nanometer-thick COF films with a practical gas-separating capability. The films were prepared using the digital alternating deposition of the precursor molecules, which guarantees a precisely controlled stoichiometry required for applying different annealing conditions for the COF-forming reactions. Under certain

annealing conditions, atomic-scale oriented network structures were observed by high resolution STEM, resulting in the higher CO_2/N_2 separation ratio. Based on the quantum chemical calculations, the CO_2 and N_2 adsorption site was the O atom of the imide group. The difference in the adsorption energies governs the role of the surface diffusion on the pore wall during the permeation. These results have provided a new practical technique for the fabrication of free-standing COF films with well-defined structures and has shed light on their gas separation applications.

We also numerically solved model equations using a dual mode sorption model and partial immobilization model along with a finite differential model. By adjusting the solution parameters to the experimental data, the appropriate model parameters of COF films were determined and we found that the solubility selectivity mainly contributed to the permselectivity.

The alternating digital deposition polymerization opens a new avenue for an efficient process of fabricating practical COF films and their applications as gas separation membranes.

Supporting Information

Details of gas permeation model analysis, DFT calculation, schematic illustration of the apparatus for the gas permeation experiments, decrease in the QCM frequency during the alternating deposition, FT-IR spectrum of the precursor molecules and films, laser microscope images of the exfoliated films, HR-STEM images of the LTA-COF film, thickness of the HTA- and LTA- COF films, chemical stabilities for the HTA-COF films, CO_2 and N_2 gas permeances of the HTA-COF films, LTA-COF films and a Al_2O_3 support and pressure dependence of the CO_2/N_2 separation factor and CO_2/N_2 ideal selectivity for the HTA-COF film.

Author Information

Corresponding Authors

*Email: takashi.yanase@sci.toho-u.ac.jp

*Email: shimadat@eng.hokudai.ac.jp

Notes

The authors declare no competing financial interest.

Acknowledgement

The present study was partially funded by the JST-ASTEP program (JPMJTM20JF). The instrumental analyses were supported by the Nanotechnology Initiative, MEXT, Japan. The computations were performed using the Research Center for Computational Science, Okazaki, Japan and Supercomputer Center of ISSP, The University of Tokyo.

References

(1) Cuéllar-Franca, R. M.; Azapagic, A. Carbon Capture, Storage and Utilisation Technologies: A Critical Analysis and Comparison of Their Life Cycle Environmental Impacts. *J. CO2 Util.* **2015**, *9*, 82–102. DOI: 10.1016/j.jcou.2014.12.001.

(2) Bernardo, P.; Drioli, E.; Golemme, G. Membrane Gas Separation: A Review/State of the Art. *Ind. Eng. Chem. Res.* **2009**, *48* (10), 4638–4663. DOI: 10.1021/ie8019032.

(3) Robeson, L. M. Correlation of Separation Factor versus Permeability for Polymeric Membranes. *J. Memb. Sci.* **1991**, *62* (2), 165–185. DOI: 10.1016/0376-7388(91)80060-J.

(4) Robeson, L. M. The Upper Bound Revisited. *J. Memb. Sci.* **2008**, *320* (1–2), 390–400. DOI: 10.1016/j.memsci.2008.04.030.

(5) Du, N.; Park, H. B.; Dal-Cin, M. M.; Guiver, M. D. Advances in High Permeability Polymeric Membrane Materials for CO 2 Separations. *Energy Environ. Sci.* **2012**, *5* (6), 7306–7322. DOI: 10.1039/c1ee02668b.

(6) Sanaeepur, H.; Ebadi Amooghin, A.; Bandehali, S.; Moghadassi, A.; Matsuura, T.; Van der Bruggen, B. Polyimides in Membrane Gas Separation: Monomer's Molecular Design and Structural Engineering. *Prog. Polym. Sci.* **2019**, *91*, 80–125. DOI: 10.1016/j.progpolymsci.2019.02.001.

(7) Muldoon, P. F.; Venna, S. R.; Gidley, D. W.; Baker, J. S.; Zhu, L.; Tong, Z.; Xiang, F.; Hopkinson, D. P.; Yi, S.; Sekizkardes, A. K.; Rosi, N. L. Mixed Matrix Membranes from a Microporous Polymer Blend and Nanosized Metal-Organic Frameworks with Exceptional CO2/N2Separation Performance. *ACS Mater. Lett.* **2020**, *2* (7), 821–828. DOI: 10.1021/acsmaterialslett.0c00156.

(8) Roh, E.; Subiyanto, I.; Choi, W.; Park, Y. C.; Cho, C. H.; Kim, H. CO2/N2 and O2/N2 Separation Using Mixed-Matrix Membranes with MOF-74 Nanocrystals Synthesized Via Microwave Reactions. *Bull. Korean Chem. Soc.* **2021**, *42* (3), 459–462. DOI: 10.1002/bkcs.12217.

(9) Tomita, T.; Nakayama, K.; Sakai, H. Gas Separation Characteristics of DDR Type Zeolite Membrane. *Microporous Mesoporous Mater.* **2004**, *68* (1–3), 71–75. DOI: 10.1016/j.micromeso.2003.11.016.

(10) van den Bergh, J.; Tihaya, A.; Kapteijn, F. High Temperature Permeation and Separation Characteristics of an All-Silica DDR Zeolite Membrane. *Microporous Mesoporous Mater.* **2010**, *132* (1–2), 137–147. DOI: 10.1016/j.micromeso.2010.02.011.

(11) Chen, D.; Ying, W.; Guo, Y.; Ying, Y.; Peng, X. Enhanced Gas Separation through Nanoconfined Ionic Liquid in Laminated MoS2 Membrane. *ACS Appl. Mater. Interfaces.* **2017**, *9* (50), 44251–44257. DOI: 10.1021/acsami.7b15762.

(12) Huang, K.; Liu, S.; Li, Q.; Jin, W. Preparation of Novel Metal-Carboxylate System MOF Membrane for Gas Separation. *Sep. Purif. Technol.* **2013**, *119*, 94–101. DOI: 10.1016/j.seppur.2013.09.008.

(13) Peng, Y.; Li, Y.; Ban, Y.; Yang, W. Two-Dimensional Metal–Organic Framework Nanosheets for Membrane-Based Gas Separation. *Angew. Chemie - Int. Ed.* **2017**, *56* (33), 9757–9761. DOI: 10.1002/anie.201703959.

(14) Fan, H.; Mundstock, A.; Feldhoff, A.; Knebel, A.; Gu, J.; Meng, H.; Caro, J. Covalent Organic Framework-Covalent Organic Framework Bilayer Membranes for Highly Selective Gas Separation. *J. Am. Chem. Soc.* **2018**, *140* (32), 10094–10098. DOI: 10.1021/jacs.8b05136.

(15) Fan, H.; Peng, M.; Strauss, I.; Mundstock, A.; Meng, H.; Caro, J. High-Flux Vertically Aligned 2D Covalent Organic Framework Membrane with Enhanced Hydrogen Separation. *J. Am. Chem. Soc.* **2020**, *142* (15), 6872–6877. DOI: 10.1021/jacs.0c00927.

(16) Ying, Y.; Tong, M.; Ning, S.; Ravi, S. K.; Peh, S. B.; Tan, S. C.; Pennycook, S. J.; Zhao, D. Ultrathin Two-Dimensional Membranes Assembled by Ionic Covalent Organic Nanosheets

with Reduced Apertures for Gas Separation. *J. Am. Chem. Soc.* **2020**, *142* (9), 4472–4480. DOI: 10.1021/jacs.9b13825.

(17) Ockwig, N. W.; Co, A. P.; Keeffe, M. O.; Matzger, A. J.; Yaghi, O. M. Porous , Crystalline , Covalent Organic Frameworks. *Science***.** **2005**, *310* (5751), 1166–1170. DOI: 10.1126/science.1120411

(18) Diercks, C. S.; Yaghi, O. M. The Atom, the Molecule, and the Covalent Organic Framework. *Science.* **2017**, *355* (6328), eaal1585. DOI: 10.1126/science.aal1585.

(19) Uribe-Romo, F. J.; Hunt, J. R.; Furukawa, H.; Klöck, C.; O'Keeffe, M.; Yaghi, O. M. A Crystalline Imine-Linked 3-D Porous Covalent Organic Framework. *J. Am. Chem. Soc.* **2009**, *131* (13), 4570–4571. DOI: 10.1021/ja8096256.

(20) Wu, S.; Gu, S.; Zhang, A.; Yu, G.; Wang, Z.; Jian, J.; Pan, C. A Rational Construction of Microporous Imide-Bridged Covalent-Organic Polytriazines for High-Enthalpy Small Gas Absorption. *J. Mater. Chem. A* **2015**, *3* (2), 878–885. DOI: 10.1039/c4ta04734f.

(21) Xu, T.; An, S.; Peng, C.; Hu, J.; Liu, H. Construction of Large-Pore Crystalline Covalent Organic Framework as High-Performance Adsorbent for Rhodamine B Dye Removal. *Ind. Eng. Chem. Res.* **2020**, *59* (17), 8315–8322. DOI: 10.1021/acs.iecr.0c00304.

(22) Das, P.; Mandal, S. K. In-Depth Experimental and Computational Investigations for Remarkable Gas/Vapor Sorption, Selectivity, and Affinity by a Porous Nitrogen-Rich Covalent Organic Framework. *Chem. Mater.* **2019**, *31* (5), 1584–1596. DOI: 10.1021/acs.chemmater.8b04683.

(23) Stegbauer, L.; Hahn, M. W.; Jentys, A.; Savasci, G.; Ochsenfeld, C.; Lercher, J. A.; Lotsch, B. V. Tunable Water and CO2 Sorption Properties in Isostructural Azine-Based Covalent Organic Frameworks through Polarity Engineering. *Chem. Mater.* **2015**, *27* (23), 7874–7881. DOI: 10.1021/acs.chemmater.5b02151.

(24) Zhu, T.; Pei, B.; Di, T.; Xia, Y.; Li, T.; Li, L. Thirty-Minute Preparation of Microporous Polyimides with Large Surface Areas for Ammonia Adsorption. *Green Chem.* **2020**, *22* (20), 7003–7009. DOI: 10.1039/d0gc02794d.

(25) van der Jagt, R.; Vasileiadis, A.; Veldhuizen, H.; Shao, P.; Feng, X.; Ganapathy, S.; Habisreutinger, N. C.; van der Veen, M. A.; Wang, C.; Wagemaker, M.; van der Zwaag, S.; Nagai, A. Synthesis and Structure-Property Relationships of Polyimide Covalent Organic Frameworks for Carbon Dioxide Capture and (Aqueous) Sodium-Ion Batteries. *Chem. Mater.* **2021**, *33* (3), 818–833. DOI: 10.1021/acs.chemmater.0c03218.

(26) Zhu, H. J.; Lu, M.; Wang, Y. R.; Yao, S. J.; Zhang, M.; Kan, Y. H.; Liu, J.; Chen, Y.; Li, S. L.; Lan, Y. Q. Efficient Electron Transmission in Covalent Organic Framework Nanosheets for Highly Active Electrocatalytic Carbon Dioxide Reduction. *Nat. Commun.* **2020**, *11* (1), 1–10. DOI: 10.1038/s41467-019-14237-4.

(27) Hosokawa, T.; Tsuji, M.; Tsuchida, K.; Iwase, K.; Harada, T.; Nakanishi, S.; Kamiya, K. Metal-Doped Bipyridine Linked Covalent Organic Framework Films as a Platform for Photoelectrocatalysts. *J. Mater. Chem. A.* **2021**, *9* (17), 11073–11080. DOI: 10.1039/d1ta00396h.

(28) Zhong, W.; Sa, R.; Li, L.; He, Y.; Li, L.; Bi, J.; Zhuang, Z.; Yu, Y.; Zou, Z. A Covalent Organic Framework Bearing Single Ni Sites as a Synergistic Photocatalyst for Selective

Photoreduction of CO2 to CO. *J. Am. Chem. Soc.* **2019**, *141* (18), 7615–7621. DOI: 10.1021/jacs.9b02997.

(29) Lin, S.; Diercks, C. S.; Zhang, Y. B.; Kornienko, N.; Nichols, E. M.; Zhao, Y.; Paris, A. R.; Kim, D.; Yang, P.; Yaghi, O. M.; Chang, C. J. Covalent Organic Frameworks Comprising Cobalt Porphyrins for Catalytic CO2 Reduction in Water. *Science.* **2015**, *349* (6253), 1208–1213. DOI: 10.1126/science.aac8343.

(30) Liu, J.; Han, G.; Zhao, D.; Lu, K.; Gao, J.; Chung, T. S. Self-Standing and Flexible Covalent Organic Framework (COF) Membranes for Molecular Separation. *Sci. Adv.* **2020**, *6* (41), 1–9. DOI: 10.1126/sciadv.abb1110.

(31) Dey, K.; Pal, M.; Rout, K. C.; Kunjattu, S. S.; Das, A.; Mukherjee, R.; Kharul, U. K.; Banerjee, R. Selective Molecular Separation by Interfacially Crystallized Covalent Organic Framework Thin Films. *J. Am. Chem. Soc.* **2017**, *139* (37), 13083–13091. DOI: 10.1021/jacs.7b06640.

(32) Kandambeth, S.; Biswal, B. P.; Chaudhari, H. D.; Rout, K. C.; Kunjattu H., S.; Mitra, S.; Karak, S.; Das, A.; Mukherjee, R.; Kharul, U. K.; Banerjee, R. Selective Molecular Sieving in Self-Standing Porous Covalent-Organic-Framework Membranes. *Adv. Mater.* **2017**, *29* (2), 1–9. DOI: 10.1002/adma.201603945.

(33) Zhang, Z.; Yin, C.; Yang, G.; Xiao, A.; Shi, X.; Xing, W.; Wang, Y. Stitching Nanosheets of Covalent Organic Frameworks to Build Aligned Nanopores in Nanofiltration Membranes for Precise Ion Separations. *J. Memb. Sci.* **2021**, *618*, 118754. DOI: 10.1016/j.memsci.2020.118754.

(34) Khan, N. A.; Zhang, R.; Wu, H.; Shen, J.; Yuan, J.; Fan, C.; Cao, L.; Olson, M. A.; Jiang, Z. Solid-Vapor Interface Engineered Covalent Organic Framework Membranes for Molecular Separation. *J. Am. Chem. Soc.* **2020**, 142 (31), 13450–13458. DOI: 10.1021/jacs.0c04589.

(35) Kang, Z.; Peng, Y.; Qian, Y.; Yuan, D.; Addicoat, M. A.; Heine, T.; Hu, Z.; Tee, L.; Guo, Z.; Zhao, D. Mixed Matrix Membranes (MMMs) Comprising Exfoliated 2D Covalent Organic Frameworks (COFs) for Efficient CO2 Separation. *Chem. Mater.* **2016**, *28* (5), 1277–1285. DOI: 10.1021/acs.chemmater.5b02902.

(36) Yuan, X.; Wang, Y.; Deng, G.; Zong, X.; Zhang, C.; Xue, S. Mixed Matrix Membrane Comprising Polyimide with Crystalline Porous Imide-Linked Covalent Organic Framework for N2/O2 Separation. *Polym. Adv. Technol.* **2019**, *30* (2), 417–424. DOI: 10.1002/pat.4479.

(37) Biswal, B. P.; Chaudhari, H. D.; Banerjee, R.; Kharul, U. K. Chemically Stable Covalent Organic Framework (COF)-Polybenzimidazole Hybrid Membranes: Enhanced Gas Separation through Pore Modulation. *Chem. Eur. J.* **2016**, *22* (14), 4695–4699. DOI: 10.1002/chem.201504836.

(38) Gou, X.; Zhang, Q.; Wu, Y.; Zhao, Y.; Shi, X.; Fan, X.; Huang, L.; Lu, G. Preparation and Engineering of Oriented 2D Covalent Organic Framework Thin Films. *RSC Adv.* **2016**, *6* (45), 39198–39203. DOI: 10.1039/c6ra07417k.

(39) Colson, J. W.; Woll, A. R.; Mukherjee, A.; Levendorf, M. P.; Spitler, E. L.; Shields, V. B.; Spencer, M. G.; Park, J.; Dichtel, W. R. Oriented 2D Covalent Organic Framework Thin Films on Single-Layer Graphene. *Science*. **2011**, *332* (6026), 228–232. DOI: 10.1126/science.1202747.

(40) Bisbey, R. P.; DeBlase, C. R.; Smith, B. J.; Dichtel, W. R. Two-Dimensional Covalent Organic Framework Thin Films Grown in Flow. *J. Am. Chem. Soc.* **2016**, *138* (36), 11433–11436. DOI: 10.1021/jacs.6b04669.

(41) Ratsch, M.; Ye, C.; Yang, Y.; Zhang, A.; Evans, A. M.; Börjesson, K. All-Carbon-Linked Continuous Three-Dimensional Porous Aromatic Framework Films with Nanometer-Precise Controllable Thickness. *J. Am. Chem. Soc.* **2020**, *142* (14), 6548–6553. DOI: 10.1021/jacs.9b10884.

(42) Wang, Z.; Yu, Q.; Huang, Y.; An, H.; Zhao, Y.; Feng, Y.; Li, X.; Shi, X.; Liang, J.; Pan, F.; Cheng, P.; Chen, Y.; Ma, S.; Zhang, Z. PolyCOFs: A New Class of Freestanding Responsive Covalent Organic Framework Membranes with High Mechanical Performance. *ACS Cent. Sci.* **2019**, *5* (8), 1352–1359. DOI: 10.1021/acscentsci.9b00212.

(43) Dai, W.; Shao, F.; Szczerbiński, J.; McCaffrey, R.; Zenobi, R.; Jin, Y.; Schlüter, A. D.; Zhang, W. Synthesis of a Two-Dimensional Covalent Organic Monolayer through Dynamic Imine Chemistry at the Air/Water Interface. *Angew. Chem. Int. Ed.* **2016**, *55* (1), 213–217. DOI: 10.1002/anie.201508473.

(44) Liu, K.; Qi, H.; Dong, R.; Shivhare, R.; Addicoat, M.; Zhang, T.; Sahabudeen, H.; Heine, T.; Mannsfeld, S.; Kaiser, U.; Zheng, Z.; Feng, X. On-Water Surface Synthesis of Crystalline, Few-Layer Two-Dimensional Polymers Assisted by Surfactant Monolayers. *Nat. Chem.* **2019**, *11* (11), 994–1000. DOI: 10.1038/s41557-019-0327-5.

(45) Fan, C.; Wu, H.; Guan, J.; You, X.; Yang, C.; Wang, X.; Cao, L.; Shi, B.; Peng, Q.; Kong, Y.; Wu, Y.; Khan, N. A.; Jiang, Z. Scalable Fabrication of Crystalline COF Membranes from

Amorphous Polymeric Membranes. *Angew. Chemie - Int. Ed.* **2021**, 60 (33), 18051–18058. DOI: 10.1002/anie.202102965.

(46) Gutzler, R.; Walch, H.; Eder, G.; Kloft, S.; Heckl, W. M.; Lackinger, M. Surface Mediated Synthesis of 2D Covalent Organic Frameworks: 1,3,5-Tris(4-Bromophenyl)Benzene on Graphite(001), Cu(111), and Ag(110). *Chem. Commun.* **2009**, 4456–4458. DOI: 10.1039/b906836h.

(47) Zwaneveld, N. A. A.; Pawlak, R.; Abel, M.; Catalin, D.; Gigmes, D.; Bertin, D.; Porte, L. Organized Formation of 2D Extended Covalent Organic Frameworks at Surfaces. *J. Am. Chem. Soc.* **2008**, *130* (21), 6678–6679. DOI: 10.1021/ja800906f.

(48) Joshi, T.; Chen, C.; Li, H.; Diercks, C. S.; Wang, G.; Waller, P. J.; Li, H.; Bredas, J. L.; Yaghi, O. M.; Crommie, M. F. Local Electronic Structure of Molecular Heterojunctions in a Single-Layer 2D Covalent Organic Framework. *Adv. Mater.* **2019**, *31* (3), 6–11. DOI: 10.1002/adma.201805941.

(49) Yanase, T.; Hasegawa, T.; Nagahama, T.; Shimada, T. Fabrication of Piezoelectric Polyurea Films by Alternating Deposition. *Jpn. J. Appl. Phys.* **2012**, *51*, 041603. DOI: 10.1143/JJAP.51.041603.

(50) Jiang, L.; Wang, P.; Li, M.; Zhang, P.; Li, J.; Liu, J.; Ma, Y.; Ren, H.; Zhu, G. Construction of a Stable Crystalline Polyimide Porous Organic Framework for C2H2/C2H4 and CO2/N2 Separation. *Chem. Eur. J.* **2019**, *25* (38), 9045–9051. DOI: 10.1002/chem.201900857.

(51) Mo, Y. P.; Liu, X. H.; Wang, D. Concentration-Directed Polymorphic Surface Covalent Organic Frameworks: Rhombus, Parallelogram, and Kagome. *ACS Nano.* **2017**, *11* (11), 11694–11700. DOI: 10.1021/acsnano.7b06871.

(52) Liu, X. H.; Guan, C. Z.; Ding, S. Y.; Wang, W.; Yan, H. J.; Wang, D.; Wan, L. J. On-Surface Synthesis of Single-Layered Two-Dimensional Covalent Organic Frameworks via Solid-Vapor Interface Reactions. *J. Am. Chem. Soc.* **2013**, *135* (28), 10470–10474. DOI: 10.1021/ja403464h.

(53) Stephans, L. E.; Myles, A.; Thomas, R. R. Kinetics of Alkaline Hydrolysis of a Polyimide Surface. *Langmuir.* **2000**, *16* (10), 4706–4710. DOI: 10.1021/la991105m.

(54) BAKER, R. W. *Membrane Technology And Applications, Third Edition*; John Wiley & Sons, Ltd, 2012.

(55) Kovvali, A. S.; Chen, H.; Sirkar, K. K. Dendrimer membranes: A CO2-selective molecular gate. *J. Am. Chem. Soc.* **2000**, *122* (31), 7594-7595. DOI: 10.1021/ja0013071.

(56) Gaussian 16, Revision C.01, Frisch, M. J.; Trucks, G. W.; Schlegel, H. B.; Scuseria, G. E.; Robb, M. A.; Cheeseman, J. R.; Scalmani, G.; Barone, V.; Petersson, G. A.; Nakatsuji, H.; Li, X.; Caricato, M.; Marenich, A. V.; Bloino, J.; Janesko, B. G.; Gomperts, R.; Mennucci, B.; Hratchian, H. P.; Ortiz, J. V.; Izmaylov, A. F.; Sonnenberg, J. L.; Williams-Young, D.; Ding, F.; Lipparini, F.; Egidi, F.; Goings, J.; Peng, B.; Petrone, A.; Henderson, T.; Ranasinghe, D.; Zakrzewski, V. G.; Gao, J.; Rega, N.; Zheng, G.; Liang, W.; Hada, M.; Ehara, M.; Toyota, K.; Fukuda, R.; Hasegawa, J.; Ishida, M.; Nakajima, T.; Honda, Y.; Kitao, O.; Nakai, H.; Vreven, T.; Throssell, K.; Montgomery, J. A., Jr.; Peralta, J. E.; Ogliaro, F.; Bearpark, M. J.; Heyd, J. J.; Brothers, E. N.; Kudin, K. N.; Staroverov, V. N.; Keith, T. A.; Kobayashi, R.; Normand, J.; Raghavachari, K.; Rendell, A. P.; Burant, J. C.; Iyengar, S. S.; Tomasi, J.; Cossi, M.; Millam, J. M.; Klene,

M.; Adamo, C.; Cammi, R.; Ochterski, J. W.; Martin, R. L.; Morokuma, K.; Farkas, O.; Foresman, J. B.; Fox, D. J. Gaussian, Inc., Wallingford CT, 2016.

(57) Fredrickson, G. H.; Helfand, E. Dual-Mode Transport of Penetrants in Glassy Polymers. *Macromolecules.* **1985**, *18* (11), 2201–2207. DOI: 10.1021/ma00153a024.

(58) Koros, W. J.; Paul, D. R.; Rocha, A. A. Carbon Dioxide Sorption and Transport in Polycarbonate. *J. polym. sci., Polym. phys. ed.* **1976**, *14* (4), 687–702. DOI: 10.1002/pol.1976.180140410

Graphical Abstract

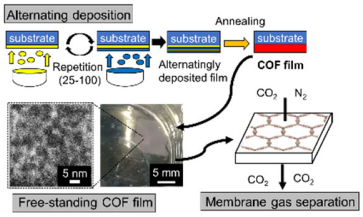

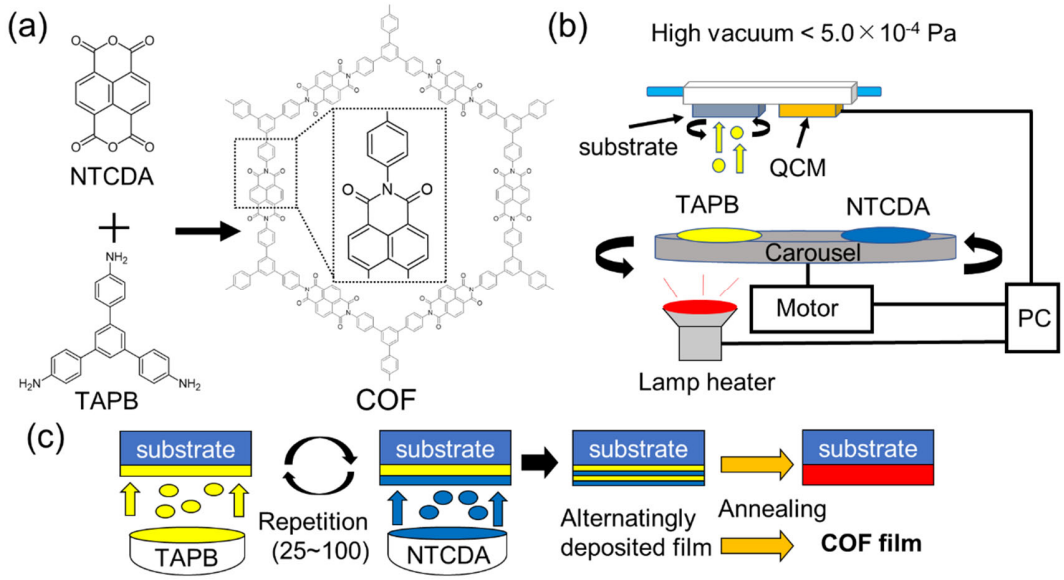

Figure 1: (a) Structure of the COF and its precursors (NTCDA and TPAB). (b) Schematic illustration of the deposition apparatus (c) Schematic illustration of alternating deposition used to prepare the COF film.

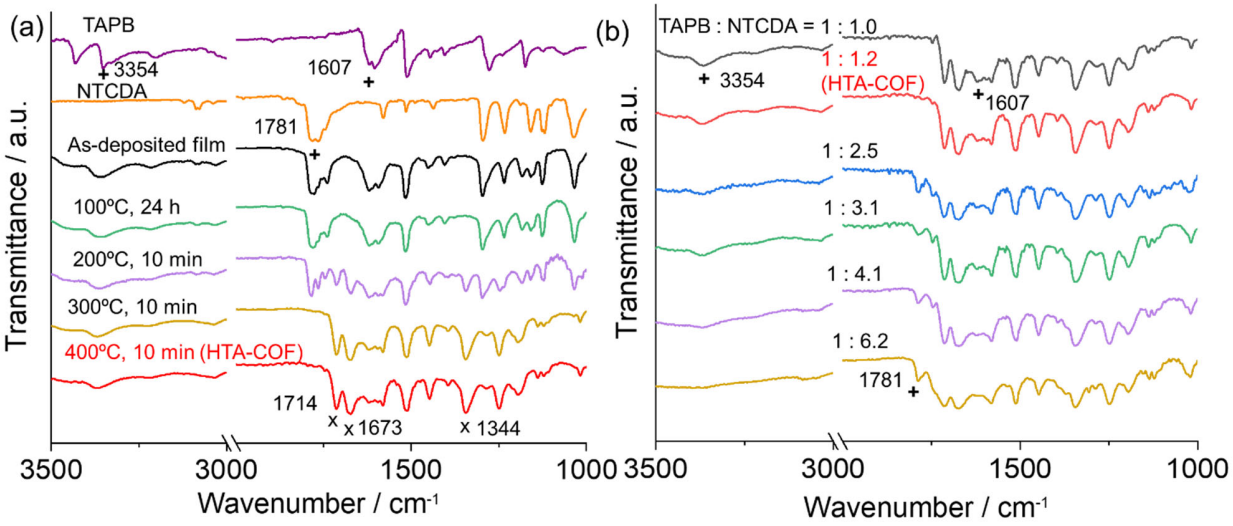

Figure 2 FTIR analyses. (a) Films prepared with TAPB : NTCDA =1 : 1.2 measured before and after vacuum annealing at various temperatures. (b) Effect of precursor ratio of the COF films annealed at 400 ºC for 10 minutes. Peaks marked with "+" correspond to precursors and those with "x" correspond to the imide group formed by polymerization.

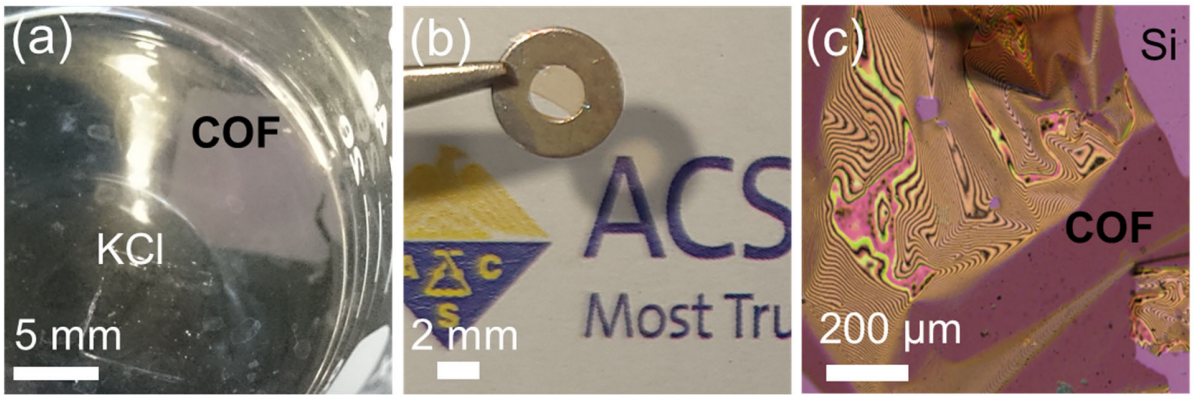

Figure 3. Free-standing COF films

(a) Optical image of a COF film floated on water by dissolving the KCl substrate.

(b) Optical image of free-standing COF film supported by a metal ring.

(c) Laser microscope image of a COF film lifted off by a Si substrate.

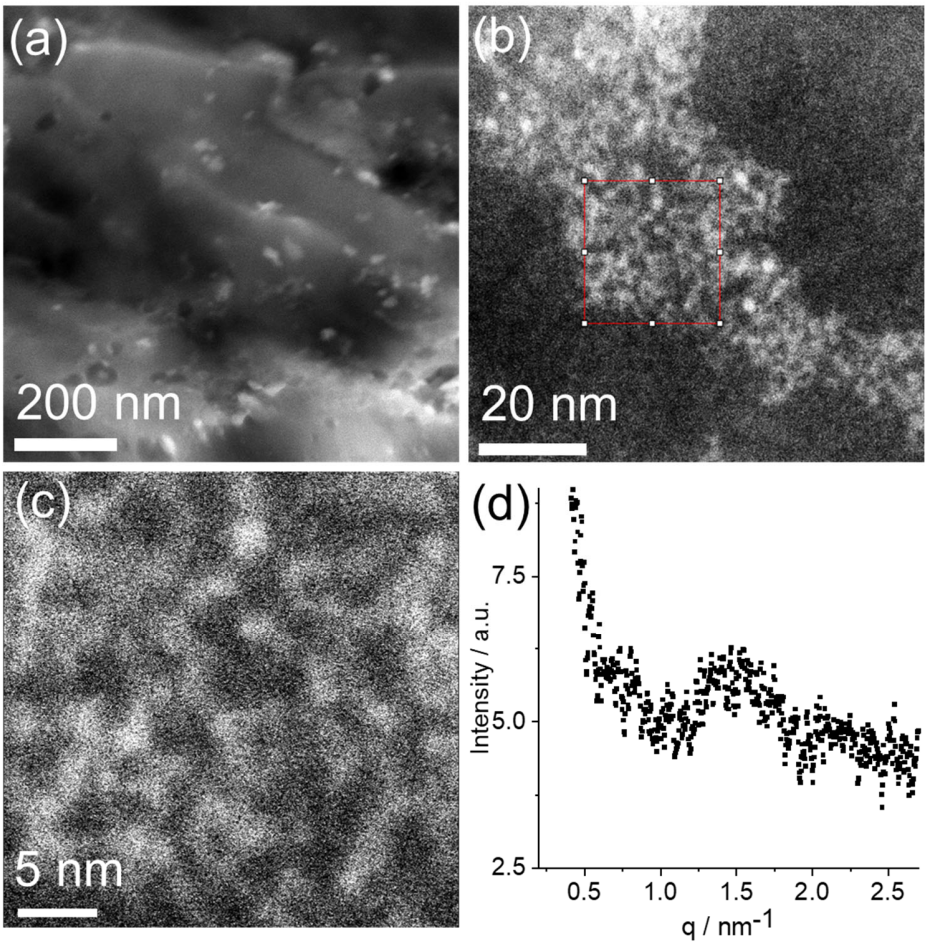

Figure 4. (a)-(c) are STEM HAADF images of an HTA-COF film at different magnifications.

(d) shows SAXS profile of an HTA-COF film.

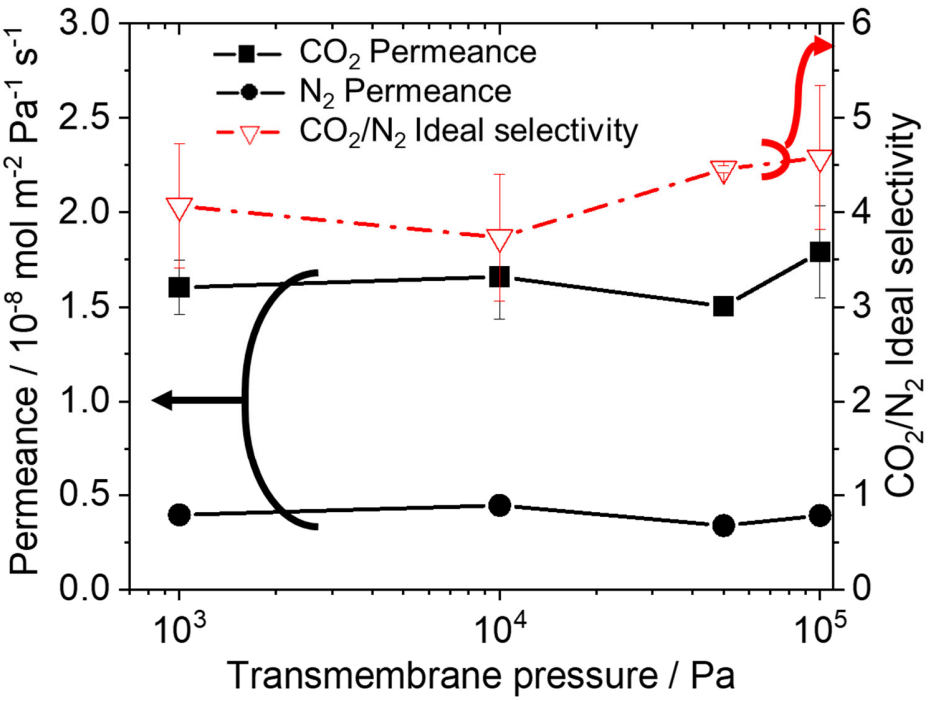

Figure 5: Gas permeation characteristics of the HTA-COF film. CO_2 and N_2 permeances and CO_2/N_2 ideal selectivity of the HTA-COF film at the transmembrane pressures of 10^3-10^5 Pa.

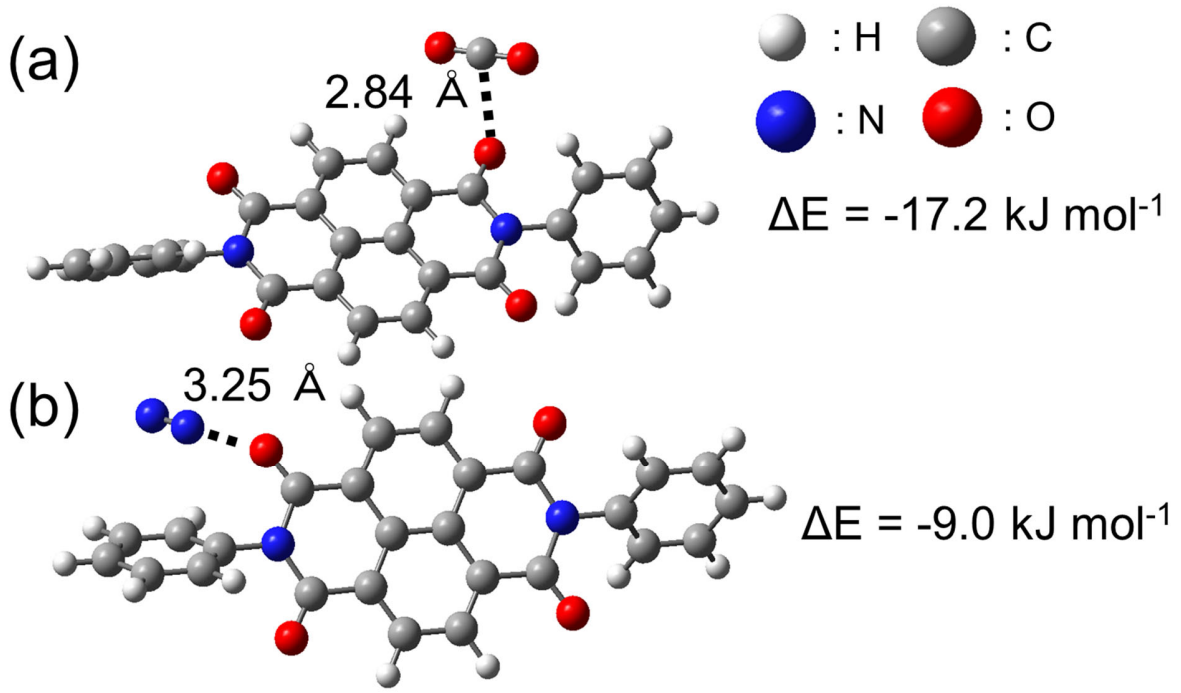

Figure 6: Optimized binding structures and binding energies for (a) CO_2 and (b) N_2 with a model partial structure of COF.

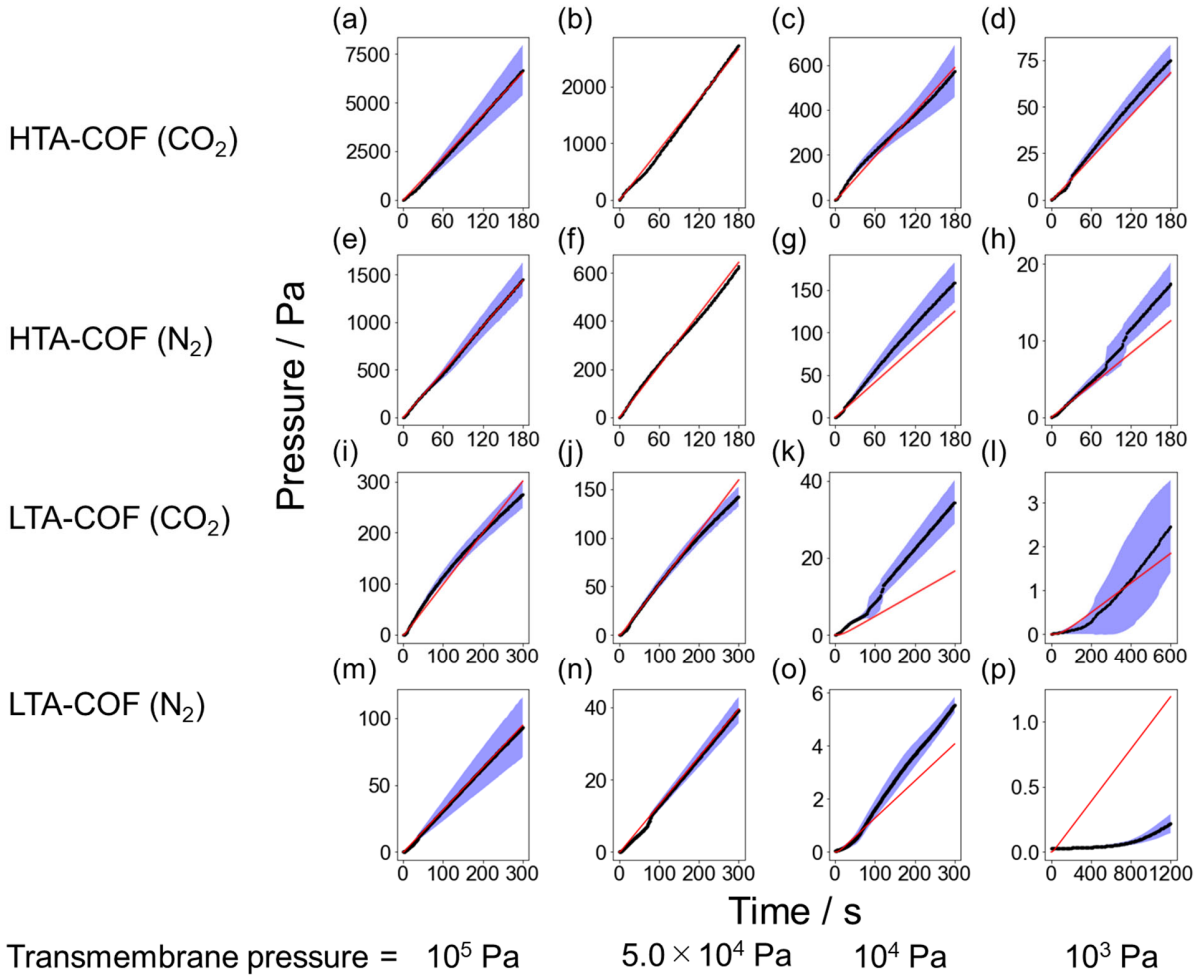

Figure7: Model fitting to the experimental gas permeation data. Black and red curves are experimental and fitting results, respectively. Blue bands show the deviation of the experimental data (repeated three times or more). (a)-(d) HTA-COF (CO_2), (e)-(h) HTA-COF (N_2), (i)-(l) LTA-COF (CO_2), (m)-(p) LTA-COF (N_2).